# Diffraction Studies of Photoexcited Crystals: Metastable Nitrosyl-Linkage Isomers of Sodium Nitroprusside

**M. D. Carducci,* M. R. Pressprich,† and P. Coppens***

*Contribution from the Department of Chemistry, Natural Sciences Complex, State University of New York at Buffalo, Buffalo, New York 14260-3000*

*Received July 25, 1996*[⊗]

**Abstract:** The geometries of two known metastable states of sodium nitroprusside dihydrate, $Na_2[Fe(CN)_5NO]\cdot 2H_2O$, and that of the ground state have been analyzed by X-ray diffraction at 50 K, a temperature at which no decay of metastable-state concentration with time is observed. Data were collected on two laser-excited crystals containing populations of ∼37% of metastable state I ($MS_1$) and ∼10% of metastable state II ($MS_2$), respectively, using imaging plates and a rotating anode source. For $MS_1$ the apparent geometry changes upon excitation, determined earlier at 138 K (Pressprich, M. R.; White, M. A.; Vekhter, Y.; Coppens, P. *J. Am. Chem. Soc.* **1994**, *116*, 5233−5238), are confirmed. However, reinterpretation of the diffraction data points to a linear, oxygen-bound isonitrosyl geometry of this species with Fe−O and N−O distances of 1.715(5) and 1.140(7) Å, respectively. The diffraction evidence points to a geometry for the $MS_2$ species in which NO is sideways bound ($\eta^2$), with Fe−N, Fe−O, and N−O distances of 1.89(2), 2.07(2), and 1.14(2) Å, respectively, compared with 1.6656(7) and 1.133(1) Å for Fe−N and N−O in the ground state. The three geometries correspond to minima in the nondissociative end-over-end linkage isomerization pathway of a diatomic molecule proposed by Armour and Taube for $N_2$ (Armor, J. N.; Taube, H. *J. Am. Chem. Soc.* **1970**, *92*, 2560−2561).

## Introduction

Although X-ray diffraction is the standard technique for the determination of ground-state molecular structure, its use for measurement of geometry changes upon exposure to a light beam is much less common. Photoirradiation can induce isomerization, dimerization, phase change, and spin-crossover, while often preserving crystallinity of the specimen.[1] The first extensive studies of photochemical reactions in the solid state were done by Schmidt and co-workers, who found the nature of the product to be frequently controlled by crystal packing, and accordingly introduced the term topochemistry.[2]

In 1977, the existence of a long-lived metastable state of sodium nitroprusside dihydrate ($Na_2[Fe(CN)_5NO]\cdot 2H_2O$, SNP (Figure 1)), produced by light irradiation at low temperature, was discovered by Mössbauer spectroscopy.[3] The color change exhibited with generation of the new state has been proposed as the basis of an information storage system, since information can be written and erased reversibly using light of two different wavelengths.[4] Similar long-lived states can be generated by irradiation of analogous nitrosyl complexes with Ru[5] or Os,[6] different ligands,[7] cations, and number of solvent molecules.[8]

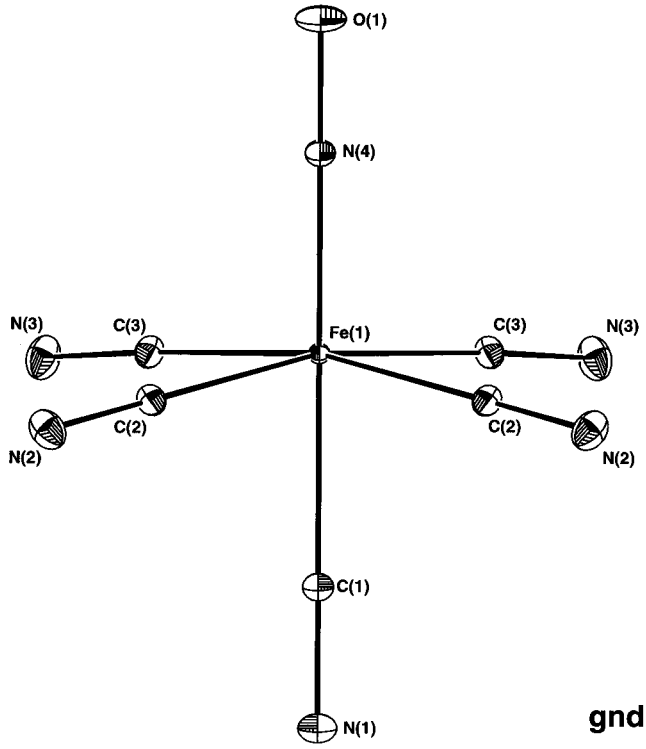


**Figure 1.** ORTEP of the ground-state SNP anion with 50% probability ellipsoids shown.

According to the classification of Enemark and Feltham,[9] in which the d-electrons are counted together with those electrons which occupy $\pi^*$ levels on the ligand, the ground state of each of these nitrosyl species is described as $\{M(NO)\}^6$. The

* Authors to whom correspondence should be addressed.

† Current address: Siemens Industrial Automation, Inc., Analytical Instrumentation, 6300 Enterprise Lane, Madison, WI 53719-1173.

⊗ Abstract published in *Advance ACS Abstracts,* March 1, 1997.

(1) Boldyreva, E. V. In *Reactivity of Solids: Past, Present and Future*; IUPAC Series on Chemistry in the 21th Century; Boldyrev, V., Ed.; Blackwell: London, 1996; pp 141−184.

(2) Cohen, M. D.; Schmidt, G. M. J. *J. Chem. Soc.* **1964**, 1996−2000. Cohen, M. D. *Angew. Chem.* **1975**, *14*, 386−393.

(3) Hauser, U.; Oestreich, V.; Rohrweck, H. D. *Z. Phys.* **1977**, *A280*, 17−25, 125−130; **1978**, *A284*, 9−19.

(4) Woike, Th.; Kirchner, W.; Schetter, G.; Barthel, Th.; Kim, H.; Haussühl, S. *Opt. Commun.* **1994**, *106*, 6−10.

(5) Woike, Th.; Haussühl, S. *Solid State Commun.* **1993**, *86*, 333−337. Woike, Th.; Zöllner, H.; Krasser, W.; Haussühl, S. *Solid State Commun.* **1990**, *73*, 149−152.

(6) Guida, J. A.; Piro, O. E.; Aymonino, P. J. *Inorg. Chem.* **1995**, *34*, 4113−4116.

(7) Ookubo, K.; Morioka, Y.; Tomizawa, H.; Miki, E. *J. Mol. Struct.* **1996**, *379*, 241−247.

(8) Zöllner, H.; Krasser, W.; Woike, Th.; Haussühl, S. *Chem. Phys. Lett.* **1989**, *161*, 497−501.

(9) Enemark, J. H.; Feltham, R. D. *Coord. Chem. Rev.* **1974**, *13*, 339−406.

S0002-7863(96)02574-7 CCC: $14.00 

phenomenon has not been detected in other metal nitrosyl complexes, with the possible exception of the {Ni(NO)}[10] compound (cyclopentadienyl)Ni(NO).[10]

Subsequent low-temperature differential scanning calorimetry (DSC)[11] and spectroscopic studies revealed a second metastable state, labeled $MS_2$. Both states can coexist in the same crystal, but with a total population always below 50%. The metastable states decay to the ground state at temperatures around 195 K ($MS_1$) and 151 K ($MS_2$). The samples studied thus contain at least two and sometimes three different species, with populations being dependent on temperature and irradiation condition.

Notwithstanding quite extensive studies, the nature of the two metastable states remains a subject of discussion, as does the reason for their extraordinarily long lifetimes at low temperature. It is usually assumed that the initial transition is an electronic excitation from the HOMO, $2b_2$ ($d_{xy}$) orbital to the LUMO, 7e ($\pi$*NO) orbital (using the approximate $C_{4v}$ point group symmetry),[12] leading to an excited complex which subsequently relaxes into two different states.[13] Raman evidence for a lowering of the N−O stretching frequency in both metastable states has been interpreted as evidence that the $\pi$*NO orbital remains occupied on relaxation. The $\pi$*NO levels would then be split by a Jahn−Teller distortion, giving rise to two states, with the higher-energy state predicted to have a linear Fe−N−O geometry and the lower-energy state a bent Fe−N−O geometry.[14] The absorption spectra of the new species have been interpreted on the basis of this model, but in more recent analyses some very low energy absorptions were reassigned to vibrational rather than electronic transitions, and an additional uninterpreted peak at ≈480 nm was revealed.[15]

The metal-to-ligand charge transfer model has been questioned by Piro and co-workers,[16] because of the weakness of the ground-state 500-nm absorption band, the direction of the Mössbauer chemical shift, the lack of splitting of vibrational modes, and the polarized IR data which do not give evidence for appreciable bending of the Fe−N−O group. They propose that $MS_1$ be assigned as $^1B_2$, corresponding to the metal configuration $6e(d_{xz},d_{yz})^4\ 2b_2(d_{xy})^1\ 5a_1(d_{z^2})^1$, which is similar to that of an $[Fe(CN)_5NO]^{3-}$ radical species generated in trace amounts by X-ray irradiation at room temperature and subsequent laser illumination. However, as pointed out by Güdel,[17] the longevity of the metastable states is inconsistent with any one-electron transfer model. Güdel argues that either a large structural change or a multielectron promotion is required to explain the stability of the species.

The identification of the metastable states must be based on the available unambiguous experimental evidence, which can be summarized as follows: (1) The generation of both metastable states requires the presence of an {MNO}[6] (M = Fe, Ru, Os) species and is not dependent on the counterion or the crystalline environment.[18] (2) Mössbauer[19] and ESR[16] evidence indicate that both metastable states are diamagnetic. (3) The Mössbauer Electric Field Gradient[19] and the lack of splitting of the cyano stretching frequencies in the Raman spectra[22] indicate that both metastable states retain the approximate $C_{4v}$ symmetry of the ground state. (4) Infrared and Raman measurements show C−N, N−O, and Fe−N stretching modes and the Fe−N−O bending mode to be downshifted on formation of the metastable states, the shifts for the modes associated with the metal−N−O group being an order of magnitude larger than the small (∼10 $cm^{-1}$) downshifts for the other vibrational frequencies.[22] However, not all observed vibrations associated with the metastable states have been assigned, nor have all expected vibrations been observed.[6] (5) Structural studies by neutron diffraction[20,21] and X-ray diffraction[14] confirm that observed changes in structure are primarily confined to the O−N−Fe−(trans)-C−N unit. The Fe−(N−O) group is essentially linear in both the ground and $MS_1$ states, in agreement with IR evidence.[22] The experiments fail to show any significant lengthening of the N−O bond, but the metal-to-ligand Fe−(NO) distance is significantly lengthened by 0.049(8) Å. (6) The spectroscopic and thermal analyses indicate that the metastable states are not populated directly, but that population occurs through a transient higher energy state, and that at least some of the $MS_1$ species is formed through the $MS_2$ state as intermediate.[13] (7) Decay of the metastable states is radiationless.[11]

We describe here 50 K X-ray diffraction studies of the ground state and both metastable states, $MS_1$ and $MS_2$, respectively, and the implication of the studies for the nature of the metastable states.

## Experimental Section

**Sample Preparation.** $Na_2[Fe(CN)_5(NO)]\cdot 2H_2O$ (Aldrich) was recrystallized from distilled water. Crystals were mounted on a Huber optical goniometer fitted with an adjustable jig holding a Dremel grinding tool. They were shortened along the *a*-axis, and two new faces with non-integer indices equal to (≈1.1 1 0) and their Friedel equivalents were introduced. By mounting the crystals with the non-integer faces perpendicular to the diffractometer $\phi$-axis, it is possible to orient the polarization vector **E** of the incident light //*c* without a crystallographic axis being aligned along the $\phi$-axis. This avoids the formation of layer lines, which causes overlap of spots on the imaging plates. A non-integer crystal face was then epoxied to a thin bundle of carbon fibers in turn held by a copper pin, which was subsequently mounted on the cold-finger of a DISPLEX cryostat colinear with the diffractometer $\phi$-axis. Freshly prepared crystals were used in each data collection. For the formation of both $MS_1$ and $MS_2$, the irradiation procedure of Rüdlinger *et al.*[20] was followed with slight modifications. In both cases the crystal was initially excited with an Omnichrome series 543 $Ar^+$ laser, $\lambda = 488$ nm, at an intensity of 100 mW/cm$^2$, and with the polarization direction of the light parallel to the *c*-axis. To reach the diffractometer-mounted crystal, held at 50 K, the light was passed through the glass bottom of a carbon-fiber vacuum chamber.[23,24] Laser irradiation was continued until a steady-state concentration was reached, as monitored by the intensity of the excitation-sensitive (2 1 2) and (2 3 2) reflections. For the $MS_1$ experiment, the crystal was subsequently warmed to 165 K, and kept at this temperature for 5 min to eliminate the $MS_2$ excited-state component, before being recooled

(10) Chen, L. X.; Bowman, M. K.; Wang, Z.; Montana, P. A.; Norris, J. R. *J. Phys. Chem.* **1994**, *98*, 9457−9464.
(11) Zöllner, H.; Woike, Th.; Krasser, W.; Haussühl, S. *Z. Kristallogr.* **1989**, *188*, 139−153.
(12) Woike, Th.; Krasser, W.; Bechthold, P. S.; Haussühl, S. *Solid State Commun.* **1983**, *45*, 499−502; *Phys. Rev. Lett.* **1984**, *53*, 1767−1770.
(13) Woike, Th.; Krasser, W.; Zöllner, H.; Kirchner, W.; Haussühl, S. *Z. Phys. D* **1993**, *25*, 351−356.
(14) Pressprich, M. R.; White, M. A.; Vekhter, Y.; Coppens, P. *J. Am. Chem. Soc.* **1994**, *116*, 5233−5238.
(15) Zöllner, H. Jülich Report 2332, Jülich, Germany, 1989.
(16) Terrile, C.; Nascimento, O. R.; Moraes, I. J.; Castellano, E. E.; Piro, O. E.; Güida, J. A.; Aymonino, P. J. *Solid State Commun.* **1990**, *73*, 481−486.
(17) Güdel, H. U. *Chem. Phys. Lett.* **1990**, *175*, 262−266.
(18) Zöllner, H.; Krasser, W.; Woike, Th.; Haussühl, S. *Chem. Phys. Lett.* **1989**, *161*, 497−501.
(19) Woike, Th.; Kirchner, W.; Kim, H.; Haussühl, S.; Rusanov, V.; Angelov, V.; Ormandjiev, S.; Bonchev, Ts.; Schroeder, A. N. F. *Hyperfine Interact.* **1993**, *7*, 265−275.
(20) Rüdlinger, M.; Schefer, J.; Vogt, T.; Woike, Th.; Haussühl, S.; Zöllner, H. *Physica* **1992**, *B180* and *181*, 293−298.
(21) Rüdlinger, M.; Schefer, J.; Chevrier, G.; Furer, N.; Güdel, H. U.; Haussühl, S.; Heger, G.; Schweiss, P.; Vogt, T.; Woike, Th.; Zöllner, H. *Z. Phys. B* **1991**, *83*, 125−130.
(22) Güida, J. A.; Aymonino, P. J.; Piro, O. E.; Castellano, E. E. *Spectrochim. Acta* **1993**, *49A*, 535−542.
(23) XTRANS cryostat chamber, Anholt Technologies Inc., Newark, DE.
(24) White, M. A.; Pressprich, M. R.; Coppens, P.; Coppens, D. D. *J. Appl. Crystallogr.* **1994**, *27*, 727−732.

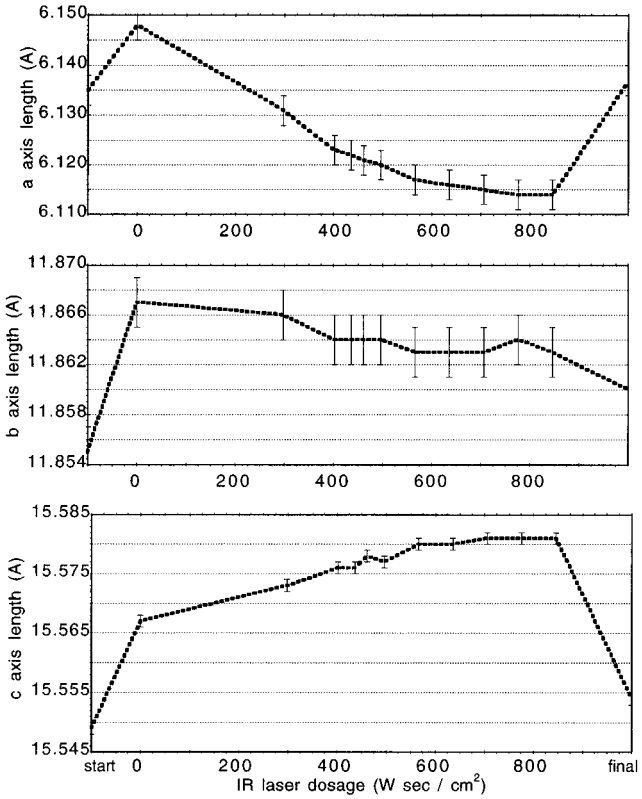


**Figure 2.** Change in crystal lattice parameters during laser illumination of SNP crystals. Ground-state cell dimensions are labeled "start". Values after saturation exposure to 488-nm light are given at the point labeled 0. IR exposure is with a wavelength of 1064 nm. The final point on the right is after saturation exposure (dose of 7760 W s/cm$^2$).

to 50 K. For the conversion to $MS_2$, the $Ar^+$ laser was subsequently replaced by a Nd-YAG laser, and illuminated at 1064 nm with a power of 70 mW/cm$^2$. At regular intervals, lattice parameters were obtained by the centering of 30 reflections.

The changes in the cell dimensions observed on generation of the $MS_2$ state are shown in Figure 2. The initial 488-nm irradiation causes an increase in all axes lengths and thus increases the volume of the cell. Upon irradiation with 1064-nm light, $MS_1$ is converted to $MS_2$ and especially along *a* the cell contracts, while the *c*-axis continues to lengthen. At the minimum of *a*, the cell volume is lower than that of the ground state. Further irradiation reduces the $MS_2$ concentration, ultimately returning all molecules to the ground state. At an integrated exposure of 7760 W s/cm$^2$, all axes lengths have returned to within three $\sigma$ of those of the ground-state crystal. Since the *a*-axis length was found to be quite sensitive to the amount of exposure, for $MS_2$ structure-determination purposes irradiation was continued until the *a* cell dimension reached a minimum at an exposure of 846 W s/cm$^2$.

**Data Collection.** All data were collected at 50 K on a four-circle Huber diffractometer using graphite-monochromated Mo K$\alpha$ radiation from a Rigaku rotating anode X-ray source (60 kV, 90 mA). The rotation method was used. FUJI imaging plates, used as detectors, were mounted in a cylindrical-segment-shaped plate holder. A specially designed antiscattering device shielded the plates from radiation scattered by the vacuum can.[25] Collection of each of the data sets required less than 20 h of X-ray exposure. Further experimental details are summarized in Table 1. No change in the excitation-sensitive reflections (2 1 2) and (2 3 2) was observed during or following data collection, nor was a change in lattice parameters indicating decay of the metastable state observed. Two additional nonsensitive high- and low-order reflections were also monitored for reference.

**Data Reduction.** The seed-skewness method was used for peak integration (program HIPPO).[26] Numerical absorption corrections were calculated with the program ABSORB,[27] while the program SORTAV[28] was used for sorting, scaling, and averaging. No time-dependent variations were observed or corrected for. Reflections measured only a single time, as well as those outliers with discordant values affecting the mean, were rejected from the data set.

**Structure Refinement.** The program package SDS was used in the least-squares refinements.[29] Additional geometry calculations and ORTEP diagrams were produced using Xtal-GX.[30] Starting positions for all atoms were taken from our previous ground-state determination. All least-squares refinements minimized the function $\sum w(|F_o| - k|F_c|)^2$, where $w = 1/(\sigma_{counting}^2(|F|) + (0.01|F|)^2)$. Anisotropic temperature parameters were applied to all non-H atoms unless noted. Scattering factors of the neutral atoms Fe, Na, O, N, C, and H (Stewart, Davidson, and Simpson model) were taken from ref 31. A single parameter was included to account for extinction effects.[32] Details of the least-squares refinements are presented in Table 2.

The $MS_1$ and $MS_2$ refinements require the inclusion of both ground-state and excited-state components, since only a fraction of the molecules in the crystal are excited. The appropriate structure factor expression is

$$F = (1 - P)F_{gs,NP} + PF_{ms,NP} + F_{rest}$$

where gs and ms represent the ground and metastable states, respectively, *P* is the metastable-state population, NP represents the nitroprusside anion, and the subscript "rest" represents the water molecules and sodium ions, which are not involved in the excitation. With gs and ms atoms in close proximity, least-squares refinement of all parameters leads to large correlations. They were eliminated by the assumption of invariance of the ground-state structure of the anion, and by using ground-state thermal parameters for the metastable-state atoms, except those of the NO group. As a result of the remaining correlation between the metastable-state population and the atomic positional parameters of the excited species, pointed out previously,[14] the excited-state population cannot be determined by refining atom occupancies, but must be obtained independently. This correlation is less severe for $MS_2$. As positional changes upon excitation are considerably larger in this case, excited-state and ground-state positions of the nitrosyl-group atoms are well separated. As a result, the excited-state population can be refined as part of the least-squares procedure.

The metastable-state population for $MS_1$ was obtained as 37% by interpolation at 488 nm between the saturation values reported in the literature from DSC measurements at 457.9 and 530.9 nm excitation wavelengths.[13] For $MS_2$, a value of 9.5(2)% was obtained by least-squares refinement. Interpolation at our 1064 nm exposure dose of 846 W s/cm$^2$ with the DSC results of Woike *et al.*[13] gives a value of 20%, indicating either that actual dosage is not exactly controllable or that cell parameters are not a simple function of population.

The fixed ground-state parameters (corrected for unit-cell changes) and the thermal parameters of the nitroprusside anion are used in the calculation of $F_{gs}$. In addition to the refinement of the scale factor and an isotropic extinction parameter, the anion is allowed to translate and rotate as a rigid body, confined to the mirror plane, to account for effects induced by the presence of the excited-state species. The total shift is small, 0.0016(3) Å in the case of $MS_1$ and 0.0031(1) Å in the case of $MS_2$. Rotation about an axis normal to the mirror plane proved to be negligible in the $MS_1$-containing crystal, and was subsequently ignored, and small, 0.25(2)°, in the case of $MS_2$.

The sodium cations and the water molecules comprising "$F_{rest}$" are assigned variable positional and thermal parameters in all refinements. No evidence for split positions was found and thermal parameters were little changed from ground-state values.

(25) Darovsky, A.; Bolotovsky, R.; Coppens, P. *J. Appl. Crystallogr.* **1994**, *27*, 1039−1040.

(26) Bolotovsky, R.; White, M. A.; Darovsky, A.; Coppens, P. *J. Appl. Crystallogr.* **1995**, *28*, 86−95.

(27) DeTitta, G. T. *J. Appl. Crystallogr.* **1985**, *18*, 75−79.

(28) Blessing, R. H. *Crystallogr. Rev.* **1987**, *1*, 3−58.

(29) Petricek, V. SDS94, System of programs for structure solution, Institute of Physics, Praha, Czech Republic, 1994.

(30) Hall, S. R.; Boulay, D. Program Xtal-GX, 1995; University of Western Australia.

(31) *International Tables for X-ray Crystallography*; Kynoch: Birmingham, England, 1974; Vol. 4.

(32) Becker, P. J.; Coppens, P. *Acta Crystallogr.* **1974**, *A30*, 129−147.

**Table 1.** Experimental Data Collection Parameters for $Na_2[Fe(CN)_5(NO)]\cdot 2H_2O$

| | ground state | $MS_1$ | $MS_2$ |
|---|---|---|---|
| space group | *Pnnm* | *Pnnm* | *Pnnm* |
| temp (K) | 50 | 50 | 50 |
| cell dimensions | | | |
| *a* (Å) | 6.136(1) | 6.148(1) | 6.115(1) |
| *b* (Å) | 11.854(1) | 11.866(1) | 11.856(1) |
| *c* (Å) | 15.555(1) | 15.554(1) | 15.571(2) |
| *V* (Å$^3$) | 1131.4(2) | 1134.7(2) | 1128.9(2) |
| *Z* | 4 | 4 | 4 |
| $d_{calcd}$ (g/cm$^3$) | 1.749 | 1.744 | 1.753 |
| abs coeff (cm$^{-1}$) | 14.1 | 14.1 | 14.1 |
| transmission factors (max/min) | 0.874/0.792 | 0.872/0.841 | 0.864/0.833 |
| crystal dimensions (mm)[a] | 0.275 × 0.275 × 0.100 | 0.125 × 0.125 × 0.125 | 0.125 × 0.125 × 0.160 |
| radiation, wavelength (Å) | | Mo Kα; $\lambda = 0.7107$ | |
| data collection method | | rotation method with imaging plates | |
| no. of plates collected | 138 | 121 | 149 |
| $((\sin\theta)/\lambda_{min} - (\sin\theta)/\lambda_{max})$ (Å$^{-1}$) | 0.11−1.07 | 0.16−1.09 | 0.13−1.10 |
| unique *hkl*; upper limit | 11, 25, 32 | 9, 25, 30 | 8, 25, 30 |
| no. of reflcns meas | 36858 | 21757 | 27428 |
| no. of symm-unique reflcns | 4264 | 3369 | 3338 |
| merging $R(I)$, $wR(I)$; $w = 1/\sigma(I)^2$ | 0.0286, 0.0336 | 0.0247, 0.0275 | 0.0224, 0.0261 |
| no. of reflcns retained for least-squares refinement | 4066 | 2717 | 2809 |
| no. of retained reflcns with $I > 3\sigma(I)$ | 3941 | 2671 | 2762 |

[a] Last dimension in direction of propagation of the laser beam.

**Table 2.** Summary of Least-Squares Results

| | ground state | $MS_1$ | | $MS_2$ |
|---|---|---|---|---|
| | | O-bound | N-bound | |
| metastable population | 0 | 0.37 (fixed) | 0.37 (fixed) | 0.095(2) |
| no. of variables | 95 | 55 | 55 | 56 |
| $R(\|F\|)$ | 0.0252 | 0.0270 | 0.0269 | 0.0269 |
| $R_w(\|F\|)$[a] | 0.0334 | 0.0366 | 0.0362 | 0.0364 |
| GOF | 1.24 | 1.54 | 1.52 | 1.66 |

[a] $w(F_{obs}) = 1/\{\sigma^2(F_{obs}) + (0.01F_{obs})^2\}$.

For $MS_1$ the initial model for the excited-state structures, $F_{ms,NP}$, was that of the ground state with free positional parameters and fixed thermal parameters. For $MS_2$ this approach was less successful, as residual peaks corresponding to metastable-state C and N atoms were close to residual peaks of similar height representing the overlap density in the CN triple bonds. This bonding density caused unreasonably short bond lengths for $MS_2$ in all cyano groups, which therefore were treated as three independent rigid bodies with identical and constant bond lengths of 1.16 Å. Test refinements in which the ground-state electron density was modeled by the aspherical-atom multipole formalism[33] did not suffer this problem, and CN bond lengths refined to 1.15−1.16 Å. In the refinements, the Fe and axial cyano group of the metastable species were restricted to the crystallographic mirror plane, while the metastable NO groups were modeled in several ways. For $MS_1$, only models with the NO group constrained to the mirror plane gave satisfactory results. For $MS_2$, only models with the group disordered across the mirror account for the observed residual peaks. Models containing conventional bent nitrosyl geometries produced *R* values more than 10% higher, and did not account for the features in the residual maps, as discussed in more detail below.

While the possibility of a disordered bent Fe−N−O structure for $MS_2$ cannot be fully ruled out on the basis of the current results, the side-bound structure is the most likely one given the diffraction evidence. We note that this structure is compatible with the geometry of related compounds, as discussed further below.

**Extended Hückel Calculations.** All molecular orbital calculations and the generation of Walsh diagrams were performed using the CACAO software package.[34] Geometries for the eleven steps of the Walsh diagram were chosen approximately equidistant along the pathway proposed by Hoffmann et al.,[35] which proceeds with the M−X−Y unit first linear (steps 1, 11), then bent (steps 2, 3 and 9, 10), then kinked (steps 4, 5 and 7, 8), and finally side bound (step 6) (see Figure 8). The $Fe(CN)_5$ fragment was given idealized $C_{4v}$ symmetry with Fe−C and C−N distances of 1.935 and 1.160 Å, respectively, and an angle between the $C_4$ axis and the Fe−CN vector of 95.5°. The N−O distance was fixed at 1.14 Å; rotation of the N−O was restricted to the C2−Fe−C3 plane. N and O positions for steps 1, 5, and 11 were taken from the ground state, $MS_2$, and $MS_1$ structures, respectively. In step 6 the Fe−N and Fe−O distances are taken as equal. A simpler model rotating the NO about its midpoint reproduces these energies, except that a plateau instead of a shallow minima in total energy is observed for the side-bound species.

## Results

**The Ground-State Structure.** The geometry of the ground state is in agreement with earlier results,[14,36,37] but is more accurate because of the lower temperature and larger number of reflections collected in the present study. The positional and isotropic thermal parameters are listed in Table 3. Bond distances and angles in the anion are listed in Table 4, while an ORTEP diagram is given in Figure 1. A representative difference map in a section containing the Fe atom, the NO, and three CN ligands, calculated with the parameters of the full-data refinement, shows bonding features in the CN, NO, and Fe−C regions (Figure 3). For less extensive data sets such features tend to disappear because the least-squares parameters will be biased such as to account for the bonding density.[38] With extensive very low-temperature data, the bias is reduced by the inclusion of large numbers of high-order reflections, and the bonding features do appear in residual density maps. The map is in agreement with earlier deformation density studies of ground-state SNP.[14,37] The background noise away from the bonding regions is low, attesting to the quality of the data.

**The Structure of $MS_2$.** A section of the difference Fourier map after the initial refinement of the rigid-body ground-state

(33) Hansen, N. K.; Coppens, P. *Acta Crystallogr.* **1978**, *A34*, 909−921. Coppens, P. *Annu. Rev. Phys. Chem.* **1992**, *43*, 663−692.

(34) Program package CACAO, PC version 4.0, July 1994. See: Mealli, C.; Proserpio, D. M. *J. Chem. Educ.* **1990**, *67*, 399−402.

(35) Hoffmann, R.; Chen, M.-L.; Thorn, D. L. *Inorg. Chem.* **1977**, *16*, 503−511.

(36) Bottomley, F.; White, P. S. *Acta Crystallogr.* **1979**, *B35*, 2193−2195. Navaza, A.; Chevrier, G.; Alzari, P. M.; Aymonino, P. J. *Acta Crystallogr.* **1989**, *C45*, 839−841.

(37) Antipin, M. Yu.; Tsirel'son, V. G.; Flyugge, M. P.; Struchkov, Yu. T.; Ozerov, R. P. *Sov. J. Coord. Chem.* **1987**, *13*, 67−75.

(38) Coppens, P.; Becker, P. In *International Tables for Crystallography*, Kluwer Academic Publishers: Dordrecht, 1992; Vol. C, Chapter 8.7, pp 627−652.

**Table 3.** Atomic Fractional Coordinates and Equivalent Isotropic Thermal Parameters (50 K) for Ground State (Top line), $MS_1$ O-Bound (Second Line), and $MS_2$ (Third Line)

| atom | *x* | *y* | *z* | $U_{iso}$ (Å$^2$) |
|---|---|---|---|---|
| Fe(1) | 0.50076(2) | 0.280393(9) | 0.5 | 0.00316(2) |
| | 0.4953(6) | 0.2781(2) | 0.5 | 0.00316[a] |
| | 0.5163(8) | 0.2852(3) | 0.5 | 0.00316 |
| N(4) | 0.7271(1) | 0.35797(6) | 0.5 | 0.0056(1) |
| | 0.8912(9) | 0.4035(3) | 0.5 | 0.0102(5)[b] |
| | 0.794(3) | 0.342(1) | 0.5313(10) | 0.014(3)[b] |
| O(1) | 0.8877(1) | 0.40510(6) | 0.5 | 0.0119(2) |
| | 0.7280(7) | 0.3579(3) | 0.5 | 0.0088(4)[b] |
| | 0.755(3) | 0.406(1) | 0.4790(7) | 0.011(2)[b] |
| C(1) | 0.2497(1) | 0.18290(7) | 0.5 | 0.0065(2) |
| | 0.2432(9) | 0.1817(3) | 0.5 | 0.0065 |
| | 0.279(2) | 0.1931(9) | 0.5 | 0.0065 |
| C(2) | 0.6074(1) | 0.17957(5) | 0.58797(4) | 0.0064(1) |
| | 0.6044(7) | 0.1774(3) | 0.5883(1) | 0.0064 |
| | 0.607(2) | 0.1824(6) | 0.5900(4) | 0.0064 |
| C(3) | 0.3458(1) | 0.36208(5) | 0.41086(4) | 0.0067(1) |
| | 0.3427(7) | 0.3614(3) | 0.4107(1) | 0.0067 |
| | 0.356(2) | 0.3664(8) | 0.4104(4) | 0.0067 |
| N(1) | 0.0991(1) | 0.12392(7) | 0.5 | 0.0093(2) |
| | 0.0942(8) | 0.1232(3) | 0.5 | 0.0093 |
| | 0.134(2) | 0.1297(9) | 0.5 | 0.0093 |
| N(2) | 0.66706(9) | 0.11964(4) | 0.64204(4) | 0.0095(1) |
| | 0.6668(7) | 0.1186(3) | 0.6420(1) | 0.0095 |
| | 0.649(2) | 0.1185(6) | 0.6439(4) | 0.0095 |
| N(3) | 0.2502(1) | 0.40572(5) | 0.35560(4) | 0.0105(1) |
| | 0.2478(7) | 0.4061(3) | 0.3559(1) | 0.0105 |
| | 0.257(2) | 0.4066(8) | 0.3548(4) | 0.0105 |
| Na(1) | 0.5 | 0.0 | 0.24596(3) | 0.00677(8) |
| | 0.5 | 0.0 | 0.24591(3) | 0.0066(1) |
| | 0.5 | 0.0 | 0.24597(3) | 0.0065(1) |
| Na(2) | 0.0 | 0.0 | 0.37813(3) | 0.00776(9) |
| | 0.0 | 0.0 | 0.37788(4) | 0.0076(1) |
| | 0.0 | 0.0 | 0.37835(3) | 0.0078(1) |
| O(2) | 0.17183(9) | 0.12251(5) | 0.26883(4) | 0.0107(1) |
| | 0.1720(1) | 0.12251(6) | 0.26852(5) | 0.0103(2) |
| | 0.1720(1) | 0.12236(5) | 0.26885(4) | 0.0104(2) |
| H(1) | 0.177(3) | 0.186(1) | 0.284(1) | 0.039(4)[b] |
| | 0.176(3) | 0.185(2) | 0.285(1) | 0.035(5)[b] |
| | 0.168(3) | 0.188(2) | 0.284(1) | 0.045(5)[b] |
| H(2) | 0.059(3) | 0.123(2) | 0.235(1) | 0.052(5)[b] |
| | 0.077(4) | 0.125(2) | 0.236(1) | 0.047(6)[b] |
| | 0.072(3) | 0.126(1) | 0.233(1) | 0.036(4)[b] |
| rigid-body parameters for excited state crystals | | | | |
| $MS_1$ Fe position | 0.5006(3) | 0.2805(1) | 0.5 | $\phi = 0.0°$ |
| $MS_2$ Fe position | 0.50126(8) | 0.28033(3) | 0.5 | $\phi = 0.25(2)°$ |

[a] Temperature parameters without standard deviations have been fixed at ground-state values. [b] Refined with isotropic thermal parameters.

anion only is presented in Figure 4. It shows a peak near Fe located in the direction of the nitrosyl group, a trough in the opposite direction, and peaks above each of the trans CN atoms displaced toward Fe, indicating that upon formation of $MS_2$ the Fe atom and the trans CN ligand are displaced in the direction of the nitrosyl group. The peaks below the equatorial cyano-group nitrogen atoms indicate that the equatorial ligands bend away from the nitrosyl position.

The remaining features of Figure 4 are indicative of the nitrosyl group in $MS_2$. They appear near the ground-state N(4) nitrogen position on both sides of the N−O bond. Corresponding minima at the ground-state N(4) and O(1) positions indicate a reorientation of the nitrosyl group atoms upon excitation. Because the section in Figure 4 contains two of the equatorial ligands, it is inclined by 45° to the crystallographic mirror plane bisecting the anion. A section perpendicular to the ground-state NO bond through the maxima (Figure 4 inset) shows the extended nature of the peaks. The distance between diagonally opposed maxima in this section is roughly 1.13 Å, a reasonable NO bond distance. Since the excited-state NO atoms are displaced from the mirror plane, the $MS_2$ nitrosyl group must

**Table 4.** Bond Lengths (Å) and Angles (deg) for Ground State, $MS_1$, and $MS_2$ (50 K)[a]

| | | excited state | |
|---|---|---|---|
| | ground state | $MS_1$ | $MS_2$ |
| | Distance | | |
| Fe(1)−N(4) | 1.6656(7) | | 1.893(19) |
| Fe(1)−O(1) | | 1.715(5) | 2.067(15) |
| Fe(1)−C(1) | 1.9257(9) | 1.926(6) | 1.820(13) |
| Fe(1)−C(2) | 1.9310(6) | 1.940(4) | 1.938(8) |
| Fe(1)−C(3) | 1.9403(6) | 1.947(4) | 1.958(8) |
| N(4)−O(1)* | 1.1331(10) | 1.140(7) | 1.14(2) |
| C(1)−N(1) | 1.1591(12) | 1.149(7) | 1.160 |
| C(2)−N(2) | 1.1603(8) | 1.154(4) | 1.160 |
| C(3)−N(3) | 1.1622(8) | 1.161(4) | 1.160 |
| | Angle | | |
| C(1)−Fe−C(2) | 84.23(3) | 85.0(2) | 81.4(4) |
| C(1)−Fe−C(3) | 84.69(2) | 85.0(2) | 84.0(4) |
| C(1)−Fe−N(4) | 176.63(4) | | 158.7(6) |
| C(1)−Fe−O(1) | | 177.1(3) | 168.3(5) |
| C(2)−Fe−C(2)* | 90.25(2) | 90.1(2) | 92.6(3) |
| C(2)−Fe−C(3) | 168.91(3) | 170.0(3) | 165.4(5) |
| C(2)−Fe−C(3)* | 88.20(2) | 88.5(1) | 86.4(3) |
| C(2)−Fe−N(4) | 93.40(2) | | 77.3(6) |
| C(2)−Fe−O(1)* | | 93.0(2) | 96.7(5) |
| C(3)−Fe−C(3)* | 91.22(3) | 91.1(2) | 90.9(4) |
| C(3)−Fe−N(4)* | 97.65(2) | | 117.3(6) |
| C(3)−Fe−O(1) | | 97.0(2) | 84.4(5) |
| Fe(1)−C(1)−N(1) | 179.78(8) | 179.3(4) | 176.6(11) |
| Fe(1)−C(2)−N(2) | 178.34(6) | 178.6(3) | 175.9(10) |
| Fe(1)−C(3)−N(3) | 176.49(6) | 176.6(3) | 174.8(8) |
| Fe(1)−N(4)−O(1)* | 176.03(7) | | 82.0(13) |
| Fe(1)−O(1)−N(4)* | | 174.9(4) | 65.1(12) |

[a] Atoms with asterisks are related to atoms without asterisks by the crystallographic mirror plane at $z = 0.5$.

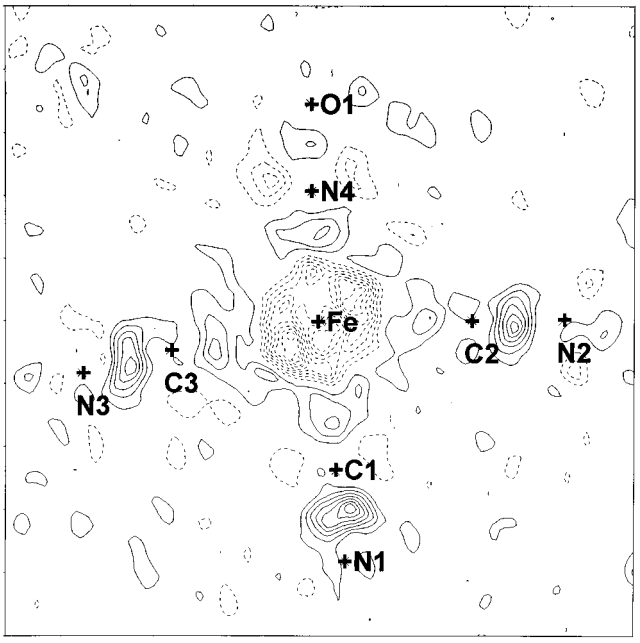


**Figure 3.** Section of the ground-state residual map containing Fe, the nitrosyl nitrogen atom, and two equatorial CN groups. The contours are at 0.1 e Å$^{-3}$, zero contour is omitted, and negative contours are indicated by broken lines. Crosses show the ground state atomic positions.

exist in at least two orientations. Subsequent least-squares refinement leads to the geometry shown in Figure 5, with a sideways-bound ($\eta^2$) NO group located in an eclipsed, rather than the stericaly less demanding staggered conformation, with respect to the equatorial ligands and with N(4) preferentially positioned over C(2).

Fractional coordinates for $MS_2$ are included in Table 3 and

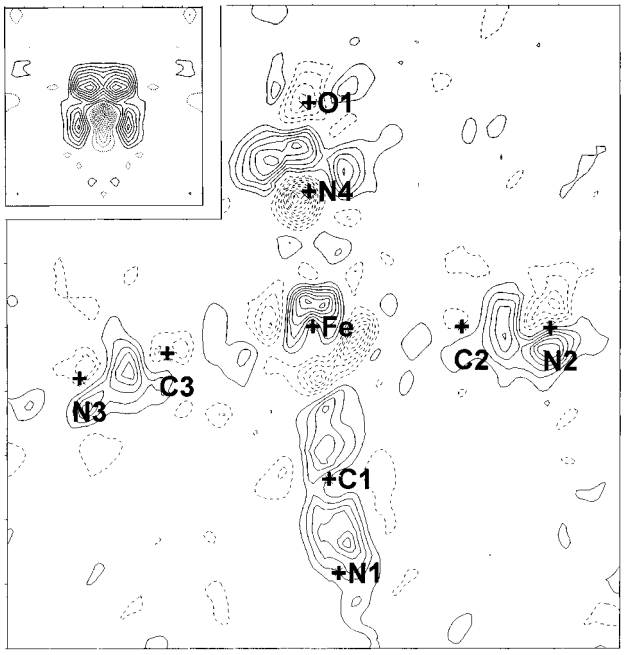


**Figure 4.** $MS_2$−ground-state difference map. The section and contours are as in Figure 3. Crosses indicate the ground-state species atomic positions. The inset shows a section perpendicular to the ground-state NO bond, containing the residual peaks.

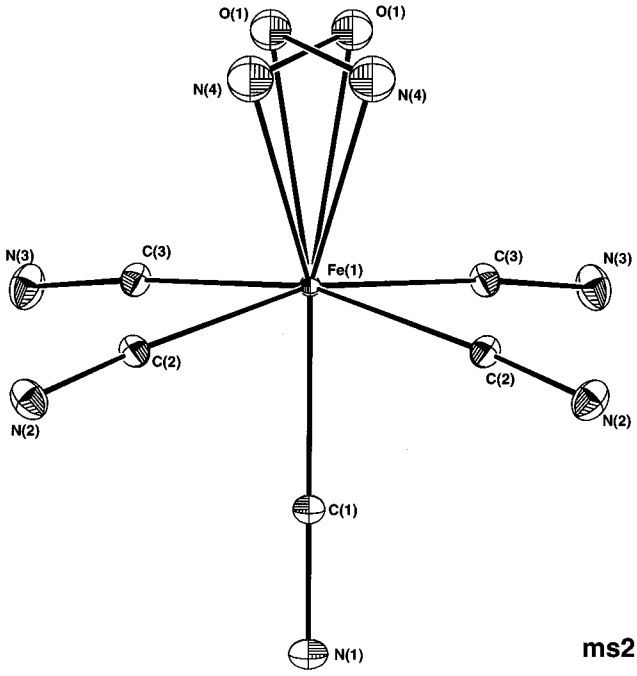


**Figure 5.** ORTEP of the $MS_2$ SNP anion. Both mirror-related NO conformations are displayed with 50% probability ellipsoids shown.

bond lengths and angles in Table 4. Excluding the NO, the anion shows little change from the tetragonal symmetry of the ground-state anion. The final difference map (Supporting Information) shows that all features are well accounted for by the model.

**The Structure of $MS_1$.** As with $MS_2$, the difference map obtained after rigid body refinement of the anion was calculated (Figure 6). The features of the map indicate a shift of the Fe atom *away* from the NO ligand and bending of the equatorial ligands *toward* the nitrosyl group, in qualitative agreement with our earlier study.[14] Least-squares refinement (labeled $MS_1$ N-bound in Table 2) reproduces the results of the previous study within experimental standard deviations, but with increased

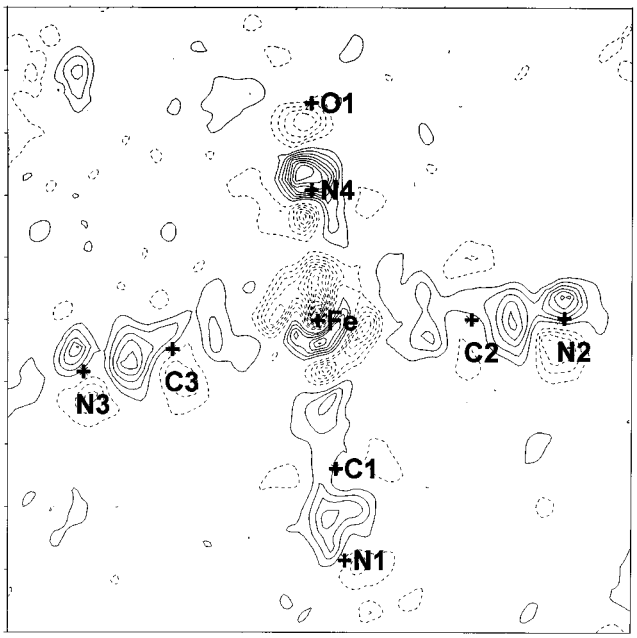


**Figure 6.** $MS_1$−ground-state difference map. The section and contours are as in Figure 3. Crosses indicate the ground-state species atomic positions.

accuracy. The most important changes upon excitation are the lengthening of the Fe−(NO) distance by 0.053(6) Å, accompanied by an increase in the C(2)−Fe−C(3) angle by 1.1(3)° to 170.0(3)°. The Fe−N−O angle and N−O bond length are not significantly changed from the ground-state values. The lack of change in the N−O bond length ($\delta = 0.003(7)$ Å), which was one of the surprising results of the 138 K study, is confirmed, making the observed decrease in N−O frequency by 115 $cm^{-1}$ even more puzzling. Badger's rule, which has been used to predict an N−O increase of 0.024 Å (over three times the experimental esd in both experiments),[21] either is not applicable in this case or the shift must be explained in an alternate way.

Since $MS_2$ appears to be a linkage isomer, the question arises if $MS_1$ might similarly have an atomic linkage different from that of the ground state. Our earlier work included a charge density analysis of the excited state. While such a study can at best be qualitative, given the mixed nature of the crystals, the excited-state valence populations on the N and O atoms of the nitrosyl group were found to be 5.9(3) and 5.0(4) electrons, an inversion in charge compared with the ground-state populations of 4.3(3) and 7.1 (3),[39] the latter being in agreement with the relative electronegativities of nitrogen and oxygen. As the excited-state electron populations were of uncertain significance, they were not commented on at the time. Nevertheless, the change in charge distribution can be explained by an inversion of the NO fragment.

To test this hypothesis we have analyzed the temperature parameters of the excited-state nitrosyl-group atoms in both the N-bound and O-bound configurations, using the current data set. The residual maps for each of these refinements are equally featureless and *R* values are essentially identical. A significant difference, however, occurs for the excited-state N and O thermal parameters. Results are summarized in Table 5. When isotropic temperature parameters of the N and O atoms are allowed to vary in the nitrosyl geometry, the resulting value for oxygen is more than four times that of the nitrogen atom. On the other hand, interchange of N and O produces very

(39) Reference 14, Supplementary Material.

**Table 5.** Isotropic "Thermal" Mean-Square Displacements $\langle u^2 \rangle$ (Å$^2$) from Least-Squares Analysis of $MS_1$

| | ground state M−NO (X-ray, 50 K) | $MS_1$ M−NO (X-ray, 50 K) | $MS_1$ M−ON (X-ray, 50 K) | ground state[a] Fe−NO (neutron, 80 K) | $MS_1$[a] Fe−NO (neutron, 80 K) |
|---|---|---|---|---|---|
| Fe | | | | | |
| proximal | 0.0056(1) | 0.0040(4) | 0.0088(5) | 0.0090(5) | 0.0139(4) |
| distal | 0.0116(1) | 0.0163(5) | 0.0102(4) | 0.0183(9) | 0.0104(5) |
| Ru | | | | | |
| proximal | 0.0072(5) | 0.004(1) | 0.008(1) | | |
| distal | 0.0141(5) | 0.022(2) | 0.015(2) | | |

[a] Equivalent isotropic mean-square displacements calculated from data in ref 20.

reasonable temperature factors, with the terminal N atom having a mean-square displacement comparable to that of the terminal oxygen atom in the ground state. This is precisely what is expected when too large an X-ray scattering factor is used for the distal atom, and too small a scattering factor for the proximal atom.

This conclusion is supported by two additional independent studies, the results of which are included in Table 5. The first is an analysis of the $MS_1$ state of the complex $K_2[Ru(NO_2)_4(NO)(OH)]$.[40] As in SNP, nitrogen and oxygen temperature parameters of the excited ruthenium species (metastable population 17%) change from physically unreasonable to normal when the NO group in $MS_1$ is inverted. The second study is the 80K neutron diffraction analysis of SNP by Rüdlinger *et al*., in which the average positions of the ground- and excited-state atoms (~0.63% ground + ~0.37% $MS_1$) were refined assuming the nitrosyl geomtry.[20,21] It is significant that the excited-state thermal parameters reported by Rüdlinger *et al*. are *higher* for the proximal than for the distal atom, while, as in the X-ray study, in the ground state they are lower for the proximal atom. The important difference between X-ray and neutron scattering is that in the X-ray case the oxygen is the more strongly scattering atom, while the situation is reversed for neutron scattering. The neutron scattering amplitude is larger for nitrogen ($b$ = 9.36 fm) than for oxygen ($b$ = 5.80 fm). Thus, in the neutron case the scattering power of the proximal atom is *over*- rather than *under*estimated when the incorrect nitrosyl geometry is used for $MS_1$, leading to the observed anomaly. This is precisely what is expected and strongly supports the X-ray results.[41]

Fractional coordinates from the isonitrosyl refinement are reported in Table 3, while the anion is pictured in Figure 7. Bond lengths and angles for the metastable anions are tabulated together with ground-state values in Table 4.

**Changes in the Unit Cell.** In the sideways-bound geometry of $MS_2$, the iron−nitrogen distance is increased from 1.6656(7) to 1.89(2) Å, while the oxygen atom is located at the much shorter distance of 2.067(15) Å from the Fe atom, compared with the nonbonded distance of ≈2.8 Å in the ground-state structure. This considerable shortening of the molecule is in agreement with the shorter *a*-axis and the somewhat higher density of the partially excited $MS_2$ crystal. The *a*-axis is most closely aligned with the ground-state Fe−N vector (~35°), and therefore most sensitive to the change in shape of the anion. In contrast, the partially excited $MS_1$ crystal shows an increase in the *a*-axis length, in qualitative agreement with the increase in the Fe−(ON) distance.

## Discussion

**The Side-On Structure of $MS_2$.** Side-on bonding of two atoms from a small molecule to a transition metal is well-known and observed for all combinations of C, N, and O. The bonding of O−N(R) nitroxide radicals and hydroxylamines to first-row transition metals, for example, occurs with metal−ligand geometric parameters similar to those we report, though the oxygen is often closer to the transition metal than the nitrogen atom.[42] Such bonding of a diatomic fragment is less common, but has come under intensive investigation.

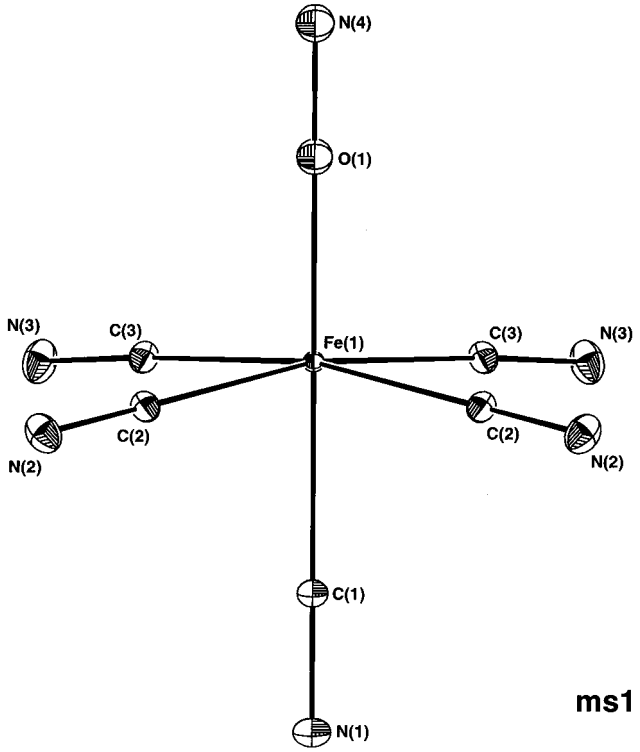


**Figure 7.** ORTEP of the $MS_1$ SNP anion with 50% probability ellipsoids shown.

Side-on bound dioxygen species have received special attention, as they are relevant for oxygen transport.[43] They are stable in, for example, $\{M(OO)\}^8$ and $\{M(OO)\}^{10}$ complexes with M = Mo, Ni, Pd, and Ir and $\{M(OO)\}^2$ and $\{M(OO)\}^4$ complexes with M = Ti and Nb. In such species $d_{xy}-\pi^*$ backbonding plays an important role, leading to weakening of the dioxygen bond and the observed eclipsed configuration of the diatomic fragment with respect to equatorial ligands.[44] Less

(40) Fomitchev, D. V.; Coppens, P. *Inorg. Chem.* **1996**, *35*, 7021−7026.

(41) For several other examples of the effect of incorrect atom assignments on the atomic displacement parameter see: Harlow, R. L. *J. Res. NIST* **1996**, *101*, 327−339.

(42) Several examples were found in a search of the Cambridge Structural Database including the following: dibromo(2,2,6,6-tetramethylpiperidinyl-1-oxy-*O*,*N*)copper(II) Cu−N = 1.997 Å and Cu−O = 1.860 Å (Caneschi, A.; Grand, A.; Laugier, J.; Rey, R.; Subra, R. *J. Am. Chem. Soc.* **1988**, *110*, 2307) and (1,1,1-tris(diphenylphosphinomethyl)ethane)(hydroxylamido-*N*,*O*)cobalt(II) tetraphenylborate, Co−N = 1.924 Å and Co−O = 1.835 Å (Vogel, S.; Huttner, G.; Zsolnai, L.; Emmerich, C. *Z. Naturforsch., Teil B* **1993**, *48*, 353).

(43) Hoffman, R.; Chen, M. M. L.; Thorn, D. L. *Inorg. Chem.* **1977**, *16*, 503.

(44) Ellinger, Y.; Latour, J. M.; Marchon, J. C.; Subra, R. *Inorg. Chem.* **1978**, *17*, 2024−2027.

**Table 6.** Geometric Differences between $MS_1$, $MS_2$, and Ground-State Nitroprusside Anions

| | $MS_1$ | | | $MS_2$ |
|---|---|---|---|---|
| | this study (50 K) | Pressprich *et al.*[14] (138 K) | Rüdlinger *et al.*[20] neutron (80 K)[a] | this study (50 K) |
| | | Distance | | |
| Fe(1)−X[b] | 0.050(5) | 0.049(8) | 0.051(6) | |
| Fe(1)−C(1) | 0.000(6) | −0.017(10) | −0.031(5) | −0.11(1) |
| Fe(1)−C(2) | 0.009(4) | 0.002(6) | −0.009(5) | 0.007(8) |
| Fe(1)−C(3) | 0.006(4) | −0.009(6) | 0.001(5) | 0.018(8) |
| N(4)−O(1) | 0.007(7) | 0.001(13) | 0.009(8) | 0.01(2) |
| C(1)−N(1) | −0.010(7) | −0.001(14) | −0.005(8) | fixed |
| C(2)−N(2) | −0.007(4) | −0.021(9) | 0.001(5) | fixed |
| C(3)−N(3) | −0.001(4) | 0.004(10) | 0.001(5) | fixed |
| | | Angle[c] | | |
| C(1)−Fe(1)−C(2) | 0.7(2) | 0.7(3) | 0.8(2) | −2.8(4) |
| C(1)−Fe(1)−C(3) | 0.4(2) | 0.8(3) | 1.1(2) | −0.7(4) |
| C(1)−Fe(1)−X | 0.5(3) | 0.6(4) | 0.5(4) | 0.3(5) |
| C(2)−Fe(1)−C(2)* | −0.1(2) | −0.1(3) | | 2.4(3) |
| C(2)−Fe(1)−C(3) | 1.1(3) | 1.6(3) | 2.0(3) | −3.6(5) |
| C(2)−Fe(1)−C(3)* | 0.3(1) | 0.5(3) | 0.2(2) | −1.8(3) |
| C(2)−Fe(1)−X | −0.4(2) | −0.3(3) | −0.5(3) | 3.1(4) |
| C(3)−Fe(1)−C(3)* | −0.2(2) | −0.3(3) | | −0.4(4) |
| C(3)−Fe(1)−X | −0.7(2) | −1.2(3) | −1.5(2) | 0.5(3) |
| Fe(1)−C(1)−N(1) | −0.5(4) | −0.7(6) | | −3.2(11) |
| Fe(1)−C(2)−N(2) | 0.3(3) | −0.3(6) | | −2.4(10) |
| Fe(1)−C(3)−N(3) | 0.1(3) | 0.0(6) | | −1.7(8) |
| Fe(1)−Nitrosyl | −1.2(4) | −2.3(8) | −0.2(6) | −94.1(13) |

[a] The parameter differences and esd's from ref 20 have been multiplied by 1/0.37, as only an average structure was refined, see ref 14 for details. [b] X represents the nitrosyl oxygen for $MS_1$ and the nitrosyl nitrogen for the ground state and for $MS_2$. [c] Atoms with asterisks are related to atoms without asterisks by a crystallographic mirror plane at $z = 0.5$.

stable side-bound dinitrogen species of Co have been detected by matrix isolation spectroscopy,[45] and using X-ray photoelectron spectroscopy, two distinct molecular states of dinitrogen assigned as the side-on and end-on species have been observed on polycrystalline iron surfaces at 85 K.[46]

The greater steric requirements of a side-bound ligand explain the observed bending of the equatorial ligands away from the nitrosyl, rather than toward the nitrosyl, as is the case for $MS_1$. The C2−Fe−C3 angle decreases by a significant 3.6(5)° to 165.4(5)° (Tables 4 and 6). The observed shortening of the trans Fe−Cl bond by 0.106(14) Å may be a result of the reduced ligand field from the side-bonded nitrosyl in the trans position. Except for the NO group, the deviations from ideal tetragonal symmetry are only about twice those found for the ground state. Nevertheless, the side-on $MS_2$ structure may be expected to give a larger value of the Mössbauer asymmetry parameter $\eta$ than has been reported ($\eta \leq 0.04$).[19] We do not have a satisfactory explanation for this discrepancy, which may be related to compensating changes in the electron density at the iron atom.

Current vibrational spectroscopy results show a decrease in the NO stretching frequency for $MS_2$ by almost 200 $cm^{-1}$ from 1950 to 1666 $cm^{-1}$,[22] indicating a weakening of the NO bond. However, there is some uncertainty in this assignment, as a band in the $MS_2$ spectrum at 1825 $cm^{-1}$, which could correspond to the NO stretching mode, remains unaccounted for.[6] As the NO in $MS_2$ shows an eclipsed conformation, larger back-donation to the $\pi^*$ orbital, as found in dioxygen complexes, would help explain the downshift in either case. The observed, though statistically insignificant, increase in the NO bond length of 0.01(2) Å may be compared with the increases of 0.064 or 0.024 Å predicted by Badger's rule,[21] if either the 1666- or the 1825-$cm^{-1}$ assignments, respectively, were correct. The reported decrease in $\nu$(FeN) by more than 100 $cm^{-1}$ is qualitatively compatible with the large increase in Fe−N distance by 0.12(2) Å. Other IR assignments involving Fe and CN are compatible with the proposed structure.

**The Isonitrosyl Structure of $MS_1$.** According to a text on metal nitrosyls[47] the isonitrosyl M−O linkage has only been structurally characterized in two cases, both of which involve the NO fragment bridging between multiple metals. The authors comment that it is surprising that no additional isonitrosyl linkages have been structurally characterized since several Lewis acid adducts are known to form via interaction of the nitrosyl oxygen with the Lewis acid. The observed increase in the Fe−(NO) bond length in $MS_1$ by 0.050(5) Å (Table 6) is in the direction expected on the basis of linkage isomerism. While distances between Fe and two-coordinate N for the compounds listed in the Cambridge Structural Data Base vary between 1.576 and 2.301 Å, those to oxygen range from 1.705 to 2.395 Å.

As is obvious from Table 6, the shape of the $MS_1$ species is very similar to that of the ground-state molecule, and distortions from tetragonal symmetry are not greater than those in the ground state. The reduction in bending of the equatorial ligands away from N−O can be understood in terms of 1−3 nonbonded interactions, in which the distance from the C(*cis*-cyano) to the proximal atom of the nitrosyl group remains approximately constant. The high symmetry structure is consistent with the very small Mössbauer asymmetry parameter $\eta$ that has been reported ($\eta \leq 0.04$).[19]

The changes in infrared spectra between this structure and the ground state would be very small, and mostly confined to the N−O, Fe−(NO), and Fe−C(axial) stretches. Only the N−O and Fe−N stretches are reported to shift substantially. The observed decrease of the NO stretching frequency from 1950 $cm^{-1}$ in the ground state to 1835 $cm^{-1}$ in $MS_1$[22] is quite similar to the 100-$cm^{-1}$ decrease observed for the analogous isomerization of $(CH_3)_3M-CN$ to $(CH_3)_3M-NC$ (M = Si or Ge).[48]

(45) Ozin, G. A.; Vander Voet, A. *Progr. Inorg. Chem.* **1975**, *19*, 105−172.

(46) Kishi, K.; Roberts, M. W. *Surf. Sci.* **1977**, *62*, 252−266. Roberts, M. W. *Chem. Soc. Rev.* **1977**, 373−391.

(47) Richter-Addo, G. R.; Legzdins, P. *Metal Nitrosyls*; Oxford University Press: New York, 1992; p 58.

(48) Nakamoto, K. *Infrared and Raman Spectra of Inorganic and Coordination Compounds*; John Wiley and Sons: New York, 1986; p 382.

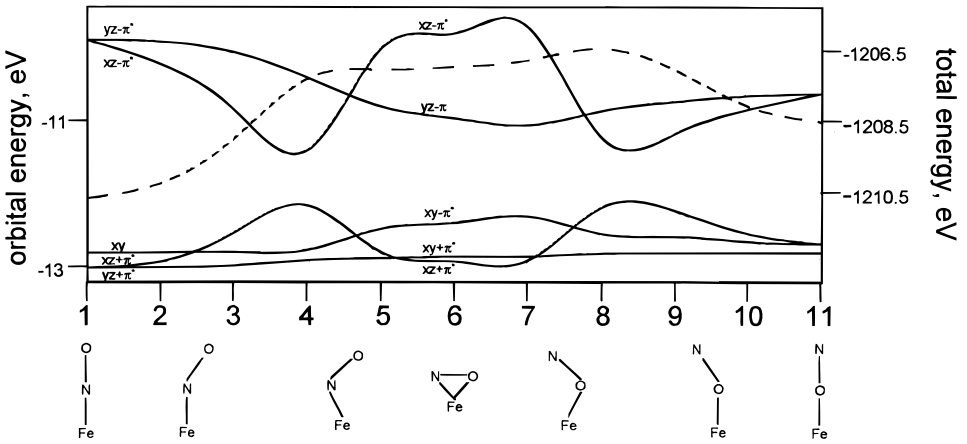


**Figure 8.** Walsh diagram of the end-to-end interconversion of nitrosyl and isonitrosyl in nitroprusside. The dotted line gives the total filled-orbital energy; solid lines give individual orbital energies. Orbital labels correspond to those used by Hoffmann *et al.*[35] Steps 1 and 11 correspond to the ground state (nitrosyl) and $MS_1$ (isonitrosyl) structures, respectively. $MS_2$ has an asymmetric $\eta^2$-NO geometry with Fe−N < Fe−O and occurs at step 5 between the kinked structure of step 4 and the symmetric Fe−N = Fe−O structure of step 6.

**Analogous Linkage Isomers and a Mechanism of Interconversion.** Continuing investigations of topochemical reactions continue to reveal new instances of linkage isomerism.[1,49,50] It is interesting to note that direct interconversion of the isomers appears limited to two families in the Enemark−Feltham notation: $\{MB\}^6$ (M = Nb, Mo, Re, Fe, Ru, Os, Co, Rh; B = $N_2$, CN, $NO_2^-$, or $SO_2$) or $\{MB\}^{10}$ (M = Si, Ge; B = CN).

Perhaps the best known examples of interconversion of linkage isomers occur for the nitrogen-bound nitro- and oxygen-bound nitrito isomers of Co(III). The prototypical example is $[Co(NH_3)_5(-NO_2)]Cl_2$. Under light irradiation, this yellow-brown compound converts to salmon pink $[Co(NH_3)_5(-ONO)]Cl_2$, which on warming or prolonged standing returns to the yellow-brown N-bound isomer. The current postulated mechanism for the low-temperature, light-induced conversion of isomers in this case[51] is (1) photoexcitation to a charge transfer state that favors rotation of the $NO_2^-$ fragment, (2) formation of a metastable intermediate with side-bound $\eta^2$ O−NO (that can be trapped at 77 K),[52] and (3) relaxation to the oxygen-bound isomer. The reverse reaction is thermodynamically driven and occurs at room temperature.

The importance of $\sigma-\pi$ rearrangements in organometallic catalysis has been emphasized in a review by Tatsumi and Tsutsui.[53] Linkage isomerization involving end-to-end rotation of dinitrogen in $[Ru(NH_3)_5N_2]Br_2$ via a side-on intermediate state was proposed by Armor and Taube, on the basis of IR studies of labeled species.[54] Recently this mechanism was confirmed by NMR studies of $(\eta^5\text{-}C_5Me_5)Re(CO)_2(N_2)$.[55] The simularities between these linkage isomerization reactions and the behavior of the SNP metastable states suggests that the same mechanism may be involved for SNP, and that the linkage isomers of SNP are formed in their ground-state electronic configurations.

Calculations of Walsh diagrams for transition metal $NO_2^-$, $SO_2$, and $NO^+$ complexes show a similarity in metal−ligand bonding in the three cases. They have been used to predict linear versus bent geometry in this series.[49,56] To examine the hypothesis on the mechanism of linkage isomerization of the nitrosyl complexes, we have used the Extended Hückel (EH) method to calculate the Walsh diagram for nitroprusside undergoing the deformation from N-bound $\eta^1$ NO, through side-bound $\eta^2$ NO, to O-bound $\eta^1$ NO. The diagram is presented in Figure 8. Five of the six molecular orbitals identified by Hoffmann et al.[35] as important to metal-diatomic bonding are included. The $z^2$-n antibonding orbital is not taken into account, as it occurs at a higher energy due to the presence of a strong trans $\sigma$-donor ligand. The remaining five orbitals show the same behavior as Hoffmann's generalized orbitals, except that the $xz\text{-}\pi^*$ orbital is substantially stabilized for bent and slightly kinked geometries. This arises from an interaction between $z^2$ and the $\pi^*$ orbital of the diatomic species, which was omitted in Hoffmann's analysis. The total electron count of these orbitals corresponds to that of the Enemark−Feltham notation.[9]

The dashed line represents the total energy for the $\{Fe(NO)\}^6$ ground-state electronic configuration (three lowest energy orbitals filled). It shows minima at the three positions along the deformation coordinate corresponding to the structures observed in this study. The diagram implies that an electronic excitation in the linear or side-bound geometries from any of the filled orbitals to the $xz\text{-}\pi^*$ orbital will produce an excited state whose equilibrium geometry is bent or slightly kinked, in agreement with excited-state Raman results of Perng and Zink.[57] It predicts the electronic absorption spectrum of the isonitrosyl species to be similar to that of the nitrosyl species in intensity and band number, but slightly lower in energy, and the side-bound species to have substantially lower energy transitions, and show a larger number of bands due to splitting of the degenerate levels, with greater intensity due to increased overlap. These predictions fully match experimental observations reported by Woike *et al.*[4] However, the EH calculation predicts $MS_1$ to be more stable than $MS_2$, while the spectroscopic and DSC results have been interpreted as favoring $MS_2$ by 0.1 eV.[11,13] In related work, a Born−Haber cycle using results from Auger spectroscopy provided an estimate of 1.33 eV for the enthalpy difference between linear N-bound and O-bound nitric oxide on a Ni surface,[58] which is comparable with the value of 1.1 eV for the difference between $MS_1$ and GS from the DSC measurements, and in qualitative agreement with the EH results.

Using the information presented above and the experimentally determined energies, a schematic diagram relating the observed

(49) Dew, V. C. Ph.D. Dissertation, University of Arkansas, Monticello, AR, 1982.
(50) Burmeister, J. L. *Coord. Chem. Rev.* **1968**, *3*, 225−245.
(51) Kubota, M.; Ohba, S. *Acta Crystallogr.* **1992**, *B48*, 627−632.
(52) Johnson, D. A.; Pashman, K. A. *Inorg. Nucl. Chem. Lett.* **1975**, *11*, 23−28.
(53) Tatsumi, K.; Tsutsui, M. *J. Mol. Catal.* **1981**, *13*, 117−145.
(54) Armor, J. N.; Taube, H. *J. Am. Chem. Soc.* **1970**, *92*, 2560−2561.
(55) Cusanelli, A.; Sutton, D. *Organometallics* **1996**, *15*, 1457−1464.
(56) Mingos, D. M. P. *Transition Met. Chem.* **1978**, *3*, 1−15.
(57) Yang, Y. Y.; Zink, J. I. *J. Am. Chem. Soc.* **1985**, *107*, 4799−4800. Perng, J. H.; Zink, J. I. *Inorg. Chem.* **1988**, *27*, 1403−1406.
(58) Egelhoff, W. F., Jr. *Phys. Rev. B* **1984**, *29*, 3681−3683.

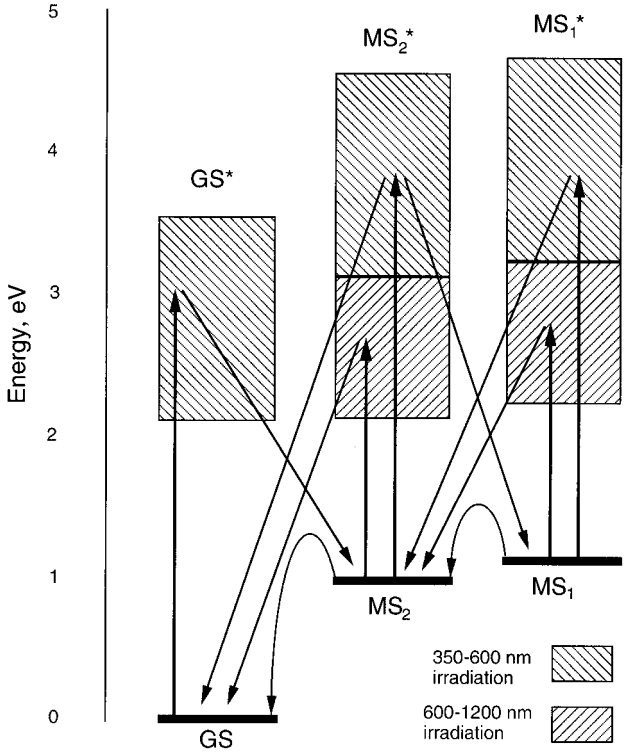


**Figure 9.** Proposed relationship and interconversion pathways between the different states of SNP. Right slanted shading indicates 350−600-nm irradiation. Left slanted shading indicates 600−1200-nm irradiation. Straight vertical arrows are electronic transitions. Slanted arrows combine an electronic transition with nuclear motion. Curved arrows are radiationless thermal decay. Energies of the various states are taken from refs 4 and 13.

species, their interconversions, and relative energies can be drawn. Such a diagram is pictured in Figure 9. Irradiation of the ground state (GS) with visible light (350−600 nm) forms GS* which can immediately decay with luminescence[59] to return to GS or with a slight nuclear motion form $MS_2$, which at temperatures below 150 K would be trapped because of the thermal barrier ($E_a = 0.5$ eV).[11] Continued irradiation in the same wavelength range allows $MS_2$ to convert to $MS_1$ which is similarly trapped at temperatures below 195 K ($E_a = 0.7$ eV). The reverse photoreactions of $MS_1$ to $MS_2$ and $MS_2$ to GS must be induced by visible light, in order to account for the observed photostationary equilibrium.[60] Irradiation with light in the range 600−1200 nm depopulates both $MS_1$ and $MS_2$, with $MS_1$ passing through $MS_2$, but has no effect on the ground state which does not absorb in this wavelength range. There is no experimental indication of the thermal decay of $MS_1$ being a two-step process, because the temperature at which the first step, $MS_1$ to $MS_2$, takes place is well above the temperature required to induce the $MS_2$ to GS deactivation. This is not the case in $Na_2[Os(CN)_5NO]\cdot 2H_2O$ in which the activation barriers are reversed and thermal transfer of $MS_1$ to $MS_2$ is observed at 200 K and $MS_2$ to GS at 220 K.[6] To our knowledge the scheme presented in Figure 9 is consistent with all reported thermodynamic and interconversion observations.

(59) Unusual and strong luminescence was reported in: Woike, Th.; Krasser, W.; Bechthold, P. S. *Solid State Commun.* **1983**, *45*, 503−506.
(60) Morioka, Y. *Solid State Commun.* **1992**, *82*, 505−507.

## Concluding Remarks

The evidence presented indicates that the metastable states of the iron and ruthenium nitrosyl complexes are linkage isomers with similar electronic configurations. While several independent experiments support the isonitrosyl structure for $MS_1$, the evidence for the side-on structure for $MS_2$ is less firm, and needs further confirmation.

Linkage isomerism provides an explanation for the long lifetime of the metastable species and their diamagnetism. The stability of the novel nitrosyl species at low temperatures indicates that similar transient reaction intermediates may play an important role in the interaction of diatomic species with metal sites as inferred for $N_2$ by Kishi and Roberts.[46] As nitric oxide binding to hemoglobin plays a key role in the regulatory mechanism involved in vasorelaxation,[61] its recombination after photolysis has been studied extensively.[62−64] The stability of the isonitrosyl and side-on nitrosyl species at low temperatures suggests that transient reaction intermediates with such geometries may play a role in the NO recombination reaction. Finally, we note that the first experimental observation of a long-lived transient species during NO recombination at low temperature has recently been reported for nitrosylcobalt Schiff bases.[65]

**Acknowledgment.** We thank Professor Paras Prasad for making the Nd-YAG laser available and Mr. David Triska for assistance. Support of this work by the National Science Foundation (CHE9021069 and CHE9317770) and the donors of the Petroleum Research Fund, administered by the American Chemical Society (PRF28664-AC3), is gratefully acknowledged.

**Supporting Information Available:** Ground-state anisotropic thermal parameters and residual maps for $MS_1$ and $MS_2$ (3 pages). See any current masthead page for ordering and Internet access information.

JA9625743

(61) Jia, L.; Bonaventura, C.; Bonaventura, J.; Stamler, J. S. *Nature* **1996**, *380*, 221−226. Perutz, M. F. *Nature* **1996**, *380*, 205.
(62) Morlino, E. A.; Walker, L. A., II; Sension, R. J.; Rodgers, M. A. *J. Am. Chem. Soc.* **1995**, *117*, 4429−4430.
(63) Traylor, T. G.; Magde, D.; Marsters, J.; Jongeward, K.; Wu, G.-Z.; Walda, K. *J. Am. Chem. Soc.* **1993**, *115*, 4808−4813.
(64) Walda, K. N.; Liu, X. Y.; Sharma, V. S.; Magde, D. *Biochemistry* **1994**, *33*, 2198−2209 and references therein.
(65) Hoshino, M.; Konishi, R.; Tezuka, N.; Ueno, I.; Seki, H. *J. Phys. Chem.* **1996**, *100*, 13569−13574.